Energy Spectrum of Ultra-high Energy Cosmic Rays with Extra-Galactic Origin

Shigeru YOSHIDA and Masahiro TESHIMA*

Department of Physics, Tokyo Institute of Technology, Tokyo 152

**Institute for Cosmic Ray Research, University of Tokyo, Tokyo 188*

We carried out a numerical calculation for the propagation of ultra-high energy cosmic ray nucleons in the intergalactic space by a Monte-Carlo method. The resulting energy spectrum above 10^{18} eV is modified by the interaction of nucleons with the micro wave background (MWB) photons, forming a bump and a cut off, with position depending on the propagation distance and source distribution. It is found that the treatment of the evolution of the universe and the interactions between cosmic rays and MWB photons is crucial. We also calculated the spectra of neutrinos and gamma rays produced by the interaction of nucleons with MWB photons. The flux of these particles strongly depends on propagation distance, cosmological evolution parameter, and the maximum energy of the cosmic rays. The possibility to detect the secondary neutrinos is also discussed.

§1. Introduction

Since the discovery of ultra-high energy cosmic rays(UHECR) ($\sim 10^{20}\ eV$), the problems of where they traveled from and how they have been accelerated remain unresolved. If UHECR are extragalactic in origin, the interactions of UHECR with the MWB photons (pair creation and pion production) give significant modifications in the energy spectrum observed on the earth[1),2)]. In this case, a cut off appears in the spectrum as an upper bound of cosmic ray energies. As UHECR propagate through intergalactic space, neutrinos and gamma rays are produced as secondary particles by photopion production. The neutrinos are decay products of the charged pions, with a typical energy of $\sim 10^{19}\ eV$ reflecting the threshold energy of pion production and the energy distribution of $\pi-\mu-e$ decay. Antielectron-neutrinos are also produced in β decay of neutrons which are produced by the charge exchange of photopion production. Photopion production produces neutral pions as well which decay into gamma rays and further produce electromagnetic cascades by interacting with the MWB radiation. UHECR also cause pair creation of secondary electrons which produce electromagnetic cascades resulting in low energy gamma rays.

Recently analytical calculations have been carried out on the propagation of UHECR in the intergalactic space by Hill and Schramm[3)] and by Berezinsky and Grigor'eva[4)]. Hill and Schramm introduced an approximation in which the evolution of MWB photons is negligible. Berezinsky and Grigor'eva utilized the transport equation under the assumption that the momentum distribution of the recoil particles due to the kinematics and fluctuations in the collision events are negligible.

In this paper, we calculate numerically the propagation of UHECR nucleons of energies from $10^{17}\ eV$ to $10^{22}\ eV$ using a Monte-Carlo method. In each interaction, we consider the kinematics carefully and we also take the cosmological evolution into account. The UHECR input spectrum is assumed to have power law behavior, and to consist of nucleons. The resultant energy spectrum is given as a function of the propagation length, and equally well by the evolution parameter. We also report on the energy spectrum of secondary neutrinos produced in the propagation of UHECR. In the calculation of muon decay processes we consider the effect of spin polarization, which leads to a slight modification in the energy spectrum of the electron-neutrinos. The electromagnetic cascade caused by interaction of the secondary gamma rays and electrons with MWB photons in intergalactic space is also calculated.

§2. Interactions of the ultra-high energy cosmic rays

UHECR lose their energy by photopion production and pair creation in the MWB photon field. Photopion production is the most important interaction for UHECR above $10^{20}\ eV$. The threshold energies of photopion

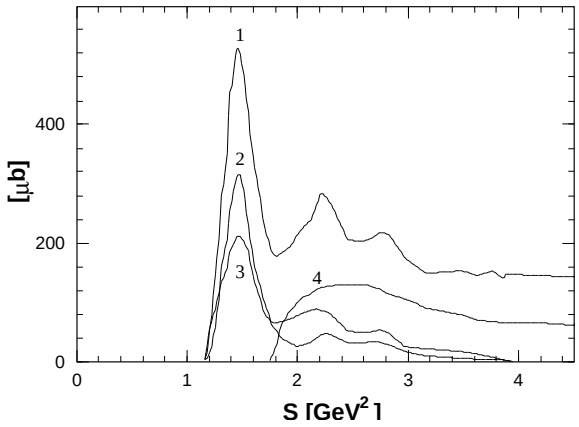

Figure 1: Cross sections for photopion production. **1** denotes the summation of all channels, **2** $\gamma p \to p\pi^0$, **3** $\gamma p \to n\pi^+$, **4** $\gamma p \to p + double\ pion$, and **5** $\gamma p \to p + triple\ pion$.

production for a photon with energy of E_γ are

$$E = \frac{(\Sigma M_\pi + M_p)^2 - M_p^2}{2E_\gamma(1+\cos\theta)}, \tag{2.1}$$

$$= 1.36 \times 10^{20}(\frac{E_\gamma}{10^{-3}eV})^{-1}(1+\cos\theta)^{-1}\ eV \qquad (\gamma\ p \to p\ \pi^0)$$

$$= 1.41 \times 10^{20}(\frac{E_\gamma}{10^{-3}eV})^{-1}(1+\cos\theta)^{-1}\ eV \qquad (\gamma\ p \to n\ \pi^+)$$

where θ is the collision angle between the photon and UHECR. The interaction of UHECR is still sizable for MWB photons with energy of $\sim 2\times10^{-3}\ eV$ where the photon energy density is 1/10 of its maximum, and the effective threshold energy of UHECR is $\sim 7 \times 10^{19}\ eV$.

The cross sections for photopion production in important channels obtained by several groups are shown in Fig.1[5]. We take account of the following channels, (a)$\gamma p \to p\pi^0$, (b)$\gamma p \to n\pi^+$, (c1)$\gamma p \to p\pi^+\pi^-$, (c2)$\gamma p \to p\pi^0\pi^0$, (c3)$\gamma p \to n\pi^+\pi^0$, (d1)$\gamma p \to p\pi^+\pi^-\pi^0$, (d2)$\gamma p \to p\pi^0\pi^0\pi^0$, (e1)$\gamma p \to n\pi^+\pi^+\pi^-$, (e2)$\gamma p \to n\pi^+\pi^0\pi^0$, (f)$\gamma p \to (p,n)\pi\pi\pi\pi$. Single pion production has a resonance structure in cross section at $s = M_p^2 + 2M_pE_\gamma \simeq 1.6\ GeV^2$, and this is the most important process for UHECR in the MWB field. Particles below $\sim 3 \times 10^{19}\ eV$ lose their energy mainly by pair creation,*i.e.* $\gamma p \to p\ e^+\ e^-$.

Fig.2 shows the energy distributions of UHECR after propagation of 1 Mpc in the MWB photon field. The input energies are $10^{18}\ eV$, $10^{19}\ eV$,

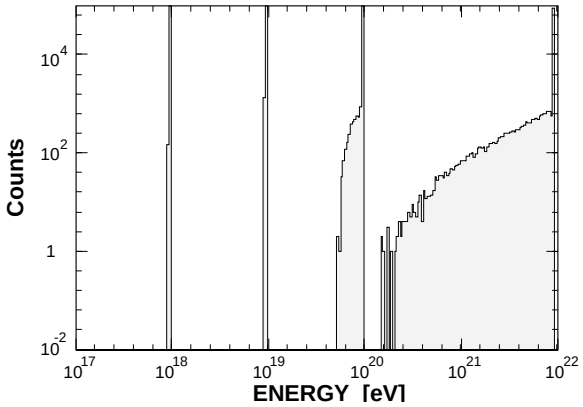

Figure 2: Energy distributions of cosmic ray nucleons after propagation of 1Mpc in the micro wave background photon field. The primary input spectra are $10^{18}eV$, $10^{19}eV$, $10^{20}eV$, and $10^{22}eV$ respectively. These spectra are obtained from our Monte-Carlo simulation of 10^5 particles in each of 4 energies.

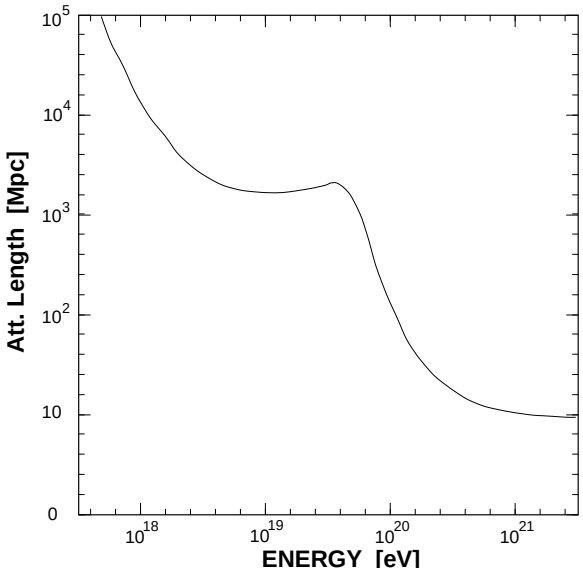

Figure 3: The attenuation length of cosmic ray nucleons in the micro wave background photon field is given. This is estimated from the 'average' amount of energy loss during travel of 1 Mpc, as shown in Fig.2, by our Monte-Carlo simulation.

$10^{20}\ eV$, and $10^{22}\ eV$ respectively. Nucleons with input energy of $10^{22}\ eV$ give a broader energy distribution after propagation than those below $10^{20}\ eV$. We can define the mean energy loss rate $-dE/dL$ and the attenuation length $\lambda = E/(-dE/dL)$. These quantities, which are based on averaging the energy loss processes, are well defined only when the propagation length is very large in comparison to the attenuation length, *i.e.* $\lambda/L << 1/10$. When the propagation length is only several times the mean free path for photopion production, careful treatment must be made. In Fig.3, we show the attenuation length, λ, obtained by our Monte-Carlo simulation.

Neutrinos and gamma rays are produced by the decay of pions. The decay process of the charged pions produced by photopion production creates electron and muon neutrinos. Electrons are also produced by pair creation of UHECR, $\gamma p \to p\ e^+\ e^-$. The decay of π^0 creates the gamma rays. These electrons and gamma rays are finally converted into lower energy gamma rays [14),15)] through an electromagnetic cascade in the intergalactic space. The main processes of this cascading are pair creation $\gamma\gamma_{bb} \to e^+e^-$ and inverse Compton scattering $e\gamma_{bb} \to e\gamma$. The higher order processes, $\gamma\gamma_{bb} \to 4e^{\pm}$ and $e\gamma_{bb} \to ee^+e^-$ only become important above $10^{19}\ eV$. The flux of these secondary particles are discussed in Sections 6 and 7.

§3. Cosmological Evolution

When UHECR propagate very long distances ($\simeq$ Gpc), the cosmological evolution of the universe becomes an important factor. We assume that our universe is an Einstain-de Sitter type. The relation between time and red shift is represented by

$$t|_z = \frac{2}{3} H_0^{-1} (1+z)^{-3/2}, \tag{3.1}$$

where H_0 is the Hubble constant. We adopt $H_0 = 75$ km sec^{-1} Mpc^{-1} in our calculation. The propagation length from the cosmic ray source to earth is given by

$$L = c(t|_{z=0} - t|_z) = \frac{2}{3}\frac{c}{H_0}\left(1 - \frac{1}{(1+z)^{3/2}}\right). \tag{3.2}$$

Therefore,we can write the infinitesimal propagation length in terms of the red shift as follows.

$$\Delta L = -\frac{c}{H_0}\frac{\Delta z}{(1+z)^{5/2}}. \tag{3.3}$$

The rate of adiabatic energy loss of UHECR due to red shift is given by

$$-\frac{dE}{dt} = H_0 (1+z)^{3/2} E. \tag{3.4}$$

Using a Friedmann-Robertson-Walker metric[18], the flux at red shift $z = 0$(time t_0) for a source where UHECR are emitted at red shift z_e (time t_e) can be represented as

$$F(E_{t_0})dE_{t_0} = \frac{\eta(t_e)n(t_e)}{4\pi R(t_0)^2 r^2}\frac{R(t_e)}{R(t_0)}\int_{E_{t_0}} dE_{t_e} G(E_{t_e}, E_{t_0}, t_e) f(E_{t_e}). \qquad (3.5)$$

Here $\eta(t_e)$ denotes the luminosity of UHECR, *i.e.*, the number density of emitted particles per source, $R(t_e)$ is the scale parameter of the universe at time t_e, $n(t_e) = n_0(R(t_0)/R(t_e))^3$ is the number density of sources, E_{t_e} is the energy of UHECR at the emission time t_e, E_{t_0} is the energy of UHECR after propagation, and $f(E_{t_e})$ is the energy spectrum at the source. $G(E_{t_e}, E_{t_0}, t_e)$ gives the energy distribution at present epoch t_0 for UHECR which were input at time t_e with energy of E_{t_e}, resulting from the energy loss due to the interactions with MWB photons and adiabatic loss described by (3.4). This quantity is calculated in the next section. The red shift z_e is related to the scale parameter $R(t_e)$ as follows.

$$1 + z_e = \frac{R(t_0)}{R(t_e)}. \qquad (3.6)$$

In the case when many sources contribute to the bulk of UHECR, the flux from them can be found by summing all the sources, according to (3.5). Specifically, we integrate each source over time and consider an isotropic distribution of sources. The total flux at our present epoch can be obtained by the volume integral,

$$J(E_{t_0})dE_{t_0} = 4\pi\int^{t_0} dt_e r^2 R(t_e)^2 (\frac{R(t_0)}{R(t_e)})^3 \frac{R(t_e)}{R(t_0)}\frac{\eta(t_e)n_0}{4\pi r^2 R(t_0)^2}\int_{E_{t_0}} dE_{t_e} G(E_{t_e}, E_{t_0}, t_e) f(E_{t_e}). \qquad (3.7)$$

$$= n_0\int^{t_0} dt_e \eta(t_e)\int_{E_{t_0}} dE_{t_e} G(E_{t_e}, E_{t_0}, t_e) f(E_{t_e}). \qquad (3.7)'$$

We assume here that the intergalactic magnetic field is negligible and UHECR propagate in a straight line.

§4. Calculation of $G(E_{t_e}, E_{t_0}, t_e)$

The propagation of UHECR is divided into steps of distance $\Delta L = c\Delta t$. In each step, the Lorentz invariant parameter s is sampled from the interaction probability:

$$\frac{dN}{dLds}(E_z, z) = \sigma(s)\frac{1}{4\pi}\int \frac{E_z + (E_z^2 - M^2)^{\frac{1}{2}}\cos\theta}{E_z}\frac{dn_\gamma}{dE_\gamma}(s, \theta, z)\frac{dE_\gamma}{ds}d\Omega, \quad (4.1)$$

where E_z is the energy of UHECR at epoch z, θ is the collision angle in the Cosmic Ray Laboratory Frame (CRLF), and E_γ is the energy of MWB photons. The number density of MWB photons is n_γ, $\sigma(s)$ is the cross section, and M is the mass of the primary UHECR. At epoch z, $dN/dLds$ can be written as

$$\frac{dN}{dLds}(E_z, z) = (1+z)^3 \frac{dN}{dLds}(E_z(1+z), 0). \tag{4.2}$$

After sampling s, the recoil energy of UHECR is determined. The energies of the secondary pions and the epoch when they are produced are recorded to study the secondary neutrinos and the gamma rays. For pair creation, the energies and emission angle of the electron-positron pair in the Nucleon Rest System (NRS) are sampled from the differential cross section and the recoil energy of UHECR are obtained by Lorentz transformation. Then, we calculate the value of red shift at the epoch after the propagation of ΔL. In every step of propagation time we decrease the energies of UHECR by (3.4) according to the adiabatic energy loss formula. After propagation from t_e to t_0, we obtain the final distribution of energies $G(E_{t_e}, E_{t_0}, t_e)$.

§5. Energy spectrum of the ultra-high energy cosmic rays

Now we apply the method developed in the above sections to obtain the energy spectrum of UHECR for two cases: a compact single source that contributes to the bulk of UHECR (single source model), and sources that are distributed isotropically (diffuse source model).

Spectra obtained on the earth for the single source model at different distances are shown in Fig.4. The label along each curve gives the red shift value of the source. The differential energy spectrum at the source is assumed to follow a power law with the power of -2 up to 10^{22} eV. The fluxes are normalized so that they have the same value at 10^{17} eV. The energy loss by photopion production creates the cut off, and the resulting UHECR piles up just below the threshold energy of photopion production, forming a bump. For the case of $z = 0.057$, the cut off is found at about 6×10^{19} eV and the bump is created at around 5×10^{19} eV. The energies at which the cut off and the bump appear decrease as the red shift of the sources increases. This is the effect of the evolution of the MWB photons described by (4.2), and the energy loss due to the red shift described by (3.4).

In Fig.4, the spectra calculated analytically using the continuous energy loss approximation with the mean energy loss rate, $-dE/dL$, are also shown for the cases of $z = 0.004$ and $z = 0.008$. The structures of the bump and cut off obtained by this analytic method are steeper than those obtained by our numerical calculation using a Monte-Carlo method. This is due to the effects of a spread in collision times and the energy loss by photopion production. When the propagation length is ~ 30 Mpc ($z = 0.008$) which

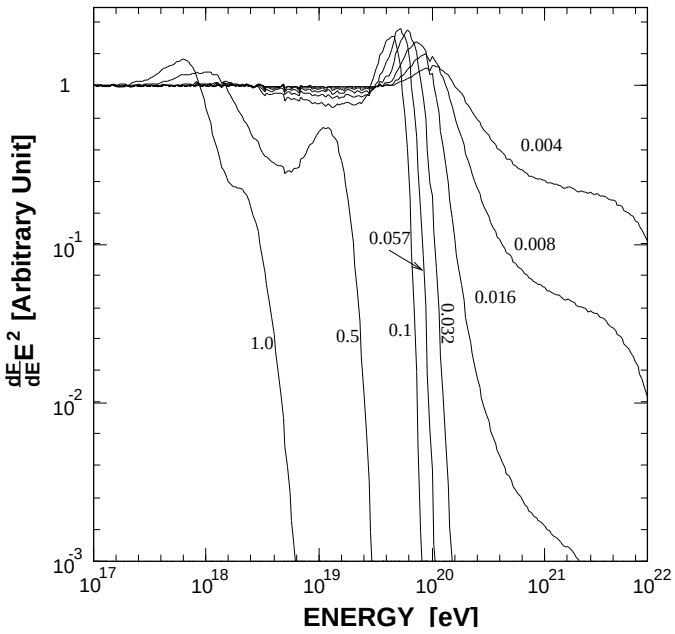

Figure 4: The spectra of a single source of ultra-high energy cosmic ray nucleons for a various red shift are shown. The primary spectra are assumed to have a power law behavior with a spectral index of 2.0. The spectra calculated analytically by the mean energy loss rate $-dE/dL$ are also shown for the cases of $z = 0.004$ and $z = 0.008$ (the broken lines).

is longer than the attenuation length of $10^{21}\ eV$ nucleons($\sim$ 10 Mpc), $\sim$ 5% of UHECR with energies higher than $\sim 10^{21}\ eV$ can reach the earth without losing their energies. However, in the analytic calculation using the continuous energy loss approximation, energies of all UHECR decrease to lower then those obtained by our full calculation. This approach necessarily introduces a lower upper bound of energies of UHECR on the earth, and there exists no UHECR above $\sim 4\times 10^{20}\ eV$ in the case of propagation of 30 Mpc. The broadening of the energy distribution of UHECR shown in Fig.2 plays an essential rule in the determination of the spectral shape and it is difficult to apply the continuous energy loss approximation to the analysis of the propagation from sources with distance of $\leq$ 100 Mpc. In cases of very long propagation distances, spectra obtained both by the Monte-Carlo simulation and analytical calculation become similar.

Some authors have argued that UHECR are accelerated in the Virgo cluster[6]. Since the red shift of the Virgo cluster is ~ 0.004, the spectrum from Virgo should have no distinct cut off. The acceleration limit at Virgo will determine the end point energy, in the simple model of no magnetic field between the Virgo cluster and the Earth.

When the source is beyond $z = 0.02$, a clear cut off should appear at energies much lower than $10^{20}\ eV$, however this is inconsistent with the observed energy spectrum[7),8)], which extends up tp $10^{20}\ eV$. The cut off energy given here is much lower than given in previous calculations[3]. This arises in a correct estimation of the evolution of MWB photons in our calculation.

Next we consider the case that the sources are distributed isotropically throughout the universe. The flux can be obtained by integrating over the sources, taking into account the effects of red shift and the evolution of the universe. Changing the integral variable from time t_e to red shift z_e in (3.7)', one obtains

$$J(E_{t_0})dE_{t_0} = n_0 \int_0^{z_{max}} dz_e \eta(z_e) \frac{1}{H_0(1+z_e)^{\frac{5}{2}}} \int_{E_{t_0}} dE_{t_e} G(E_{t_e}, E_{t_0}, z_e) f(E_{t_e}), \tag{5.1}$$

where z_{max} is the "turn-on time", *i.e.* when UHECR were created for the first time. The recent radio data[9)] indicates z_{max} is smaller than ~ 4.0. The relation between E_{t_0} and E_{t_e} is given by $G(E_{t_e}, E_{t_0}, z_e)$. Assuming the functional form of $\eta(z_e)$ is $\eta(z_e) = \eta_0(1+z_e)^m$, the integral becomes

$$J(E_{t_0})dE_{t_0} = \frac{n_0\eta_0}{H_0} \int_0^{z_{max}} dz_e (1+z_e)^{m-\frac{5}{2}} \int_{E_{t_0}} dE_{t_e} G(E_{t_e}, E_{t_0}, z_e) f(E_{t_e}) \tag{5.2}$$

in an Einstain-de Sitter universe. In this expression, $m = 0$ corresponds to the case of no evolution.

The results obtained by the integral of (5.2) for several values of m and z_{max}, are shown in Fig.5. All spectra are normalized at $10^{17}\ eV$ as before. The cut off is clear, while the sharp bump, which appeared at $\sim 6\times 10^{19}\ eV$

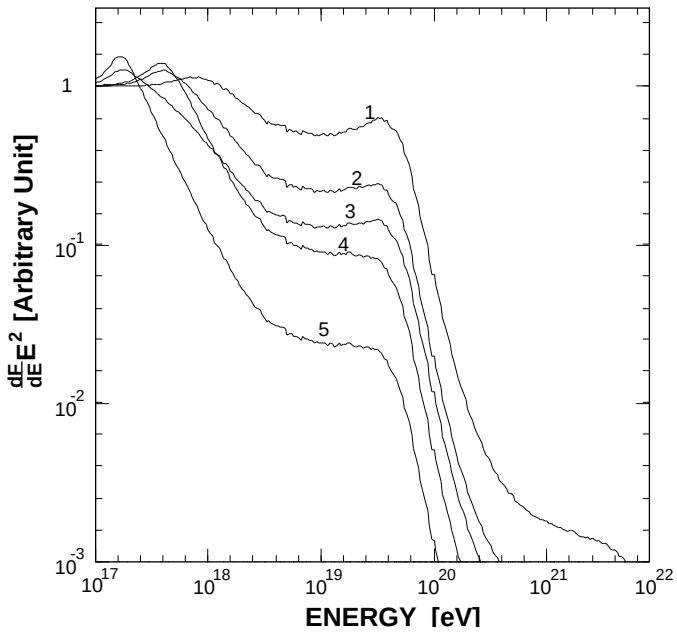

Figure 5: Diffuse source spectra of ultra-high energy cosmic ray nucleons. All of these spectra are normalized at $10^{17}\ eV$. **1** is for $(m, z_{max}) = (0.0, 2.0)$, **2** $(m, z_{max}) = (2.0, 2.0)$, **3** $(m, z_{max}) = (2.0, 4.0)$, **4** $(m, z_{max}) = (4.0, 2.0)$, and **5** $(m, z_{max}) = (4.0, 4.0)$. For the definition of m and z_{max}, please see the text.

in the case of a single source with $z < 0.1$, disappears in the case of diffuse sources. In the region between $10^{17}\ eV$ and $10^{19}\ eV$ the shape of the spectrum depends strongly on m and z_{max}, since the flux in this energy region is determined mainly by the luminosity of UHECR at the high red shift epoch. The shape of the spectrum above $10^{19}\ eV$ is almost independent of m and z_{max}. This reflects the fact that nearby sources contribute dominantly in this energy region.

§6. Energy spectrum of the secondary neutrinos

The energy distributions of decay products are obtained from the decay rate per unit time per unit energy for each decay process. The decay processes of pions and muons are treated in the NRS, and the final energies are transformed to those in the CRLF by Lorentz transformation. The spin polarization of muons as the decay products of pions is also considered in our calculation. The direction of the muon's spin in the CRLF for the running direction is given as a function of energy of the pions and muons[10], and the muon's spin polarization tends to make the electron neutrino's energy higher than the muon neutrino's energy.

Some cosmic ray protons above $\sim 10^{20}\ eV$ are converted into neutrons by photopion production (charge exchange). They decay into protons again during the long propagation producing electrons and anti-electron neutrinos. This is the mechanism for the production of anti-electron neutrinos, which creates a bulk of $\bar{\nu}_e$'s at energies $\leq 10^{17}\ eV$.

The combined fluxes of ν and $\bar{\nu}$ are shown in Fig.6 for a single source model as a function of propagation distance, alongside the spectra of UHECR for comparison. To estimate the normalization factor, we refer to the cosmic ray flux observed by the Akeno group[7], $1.9 \times 10^{-15}\ m^{-2}\,\mathrm{sec}^{-1}\,sr^{-1}$ for $E > 3 \times 10^{19}\ eV$. We assume that the observed flux of cosmic rays above $3 \times 10^{19}\ eV$ is of extra-galactic origin and consists of nucleons. The flux of neutrinos is dependent on the propagation distance especially for $E \leq 10^{18}\ eV$, while it does not depend on distance in the higher energy region.

Fig.7 shows the spectra of neutrinos for a diffuse source model. The expected spectrum of UHECR from a diffuse source is also shown for comparison. The shape and absolute value of the spectrum of neutrinos in the region below $10^{19}\ eV$ strongly depends on the evolution parameter m and on the assumption of the turn-on time z_{max}.

There is sensitivity to the value of maximum accelerated energy of UHECR in the flux of the neutrinos. Fig.8 shows the expected flux of UHECR and neutrinos for the cases that maximum accelerated energies are $10^{21}\ eV$ and $10^{22}\ eV$, respectively. The flux of neutrinos above $10^{19}\ eV$ depends strongly on the maximum energy of UHECR, while the UHECR themselves do not depend strongly on the maximum energy. The flux of these high energy neutrinos could be a probe of the maximum energy of cosmic rays at

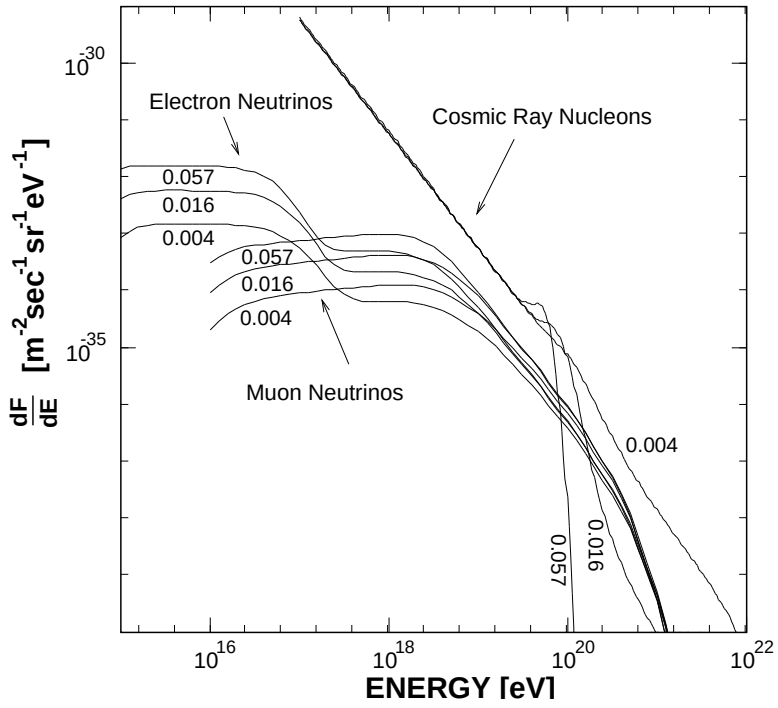

Figure 6: The single source spectra of secondary neutrinos. The red shift z is shown in this figure. The calculated spectra of cosmic ray nucleons is also shown for comparison.

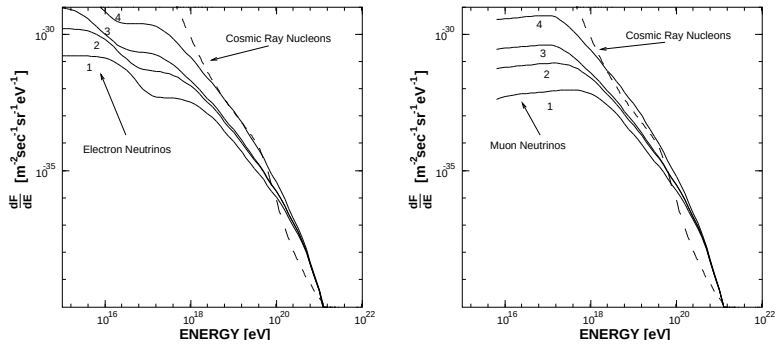

Figure 7: The diffuse source spectra of the secondary neutrinos. The calculated spectra of cosmic ray nucleons are also shown for comparison. **1** is for $(m, z_{max}) = (0.0, 2.0)$, **2** $(m, z_{max}) = (2.0, 2.0)$, **3** $(m, z_{max}) = (2.0, 4.0)$, and **4** $(m, z_{max}) = (4.0, 4.0)$.

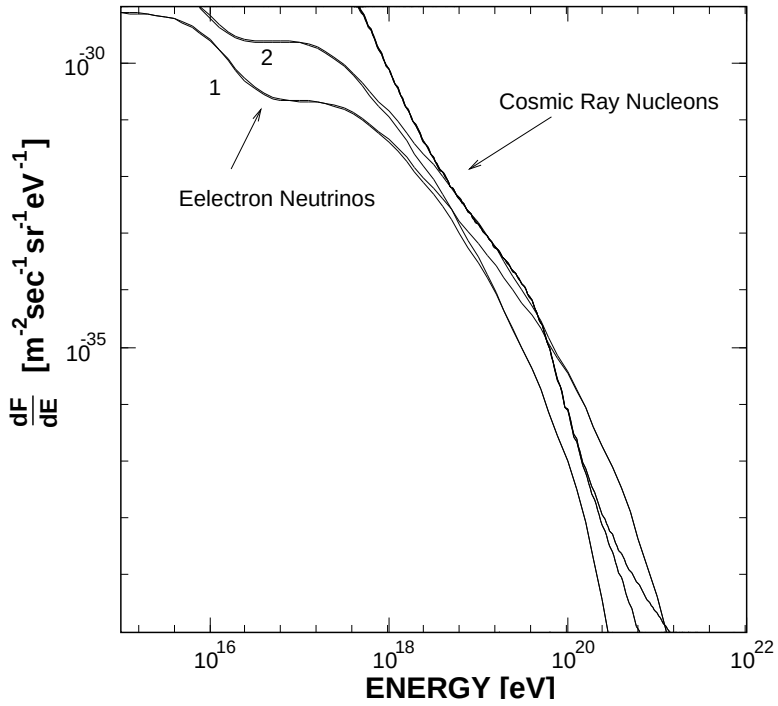

Figure 8: The expected flux of UHECR and secondary neutrinos for the maximum accelerated energy of $10^{21}eV$ and $10^{22}eV$. **1** is for $(m, z_{max}) = (4.0, 2.0)$ and **2** $(m, z_{max}) = (4.0, 4.0)$.

Table 1: The flux of the secondary neutrinos in units of $[m^{-2}\sec^{-1}sr^{-1}eV^{-1}]$

	$E=10^{18}$ eV			$E=10^{19}$ eV			$E=10^{20}$ eV			$E=10^{20}$ eV		
	Emax=10^{22} eV			Emax=10^{22} eV			Emax=10^{22} eV			Emax=10^{21} eV		
ORIGIN	UHECR	ν e	$\nu\mu$	UHECR	ν e	$\nu\mu$	UHECR	ν e	$\nu\mu$	UHECR	ν e	$\nu\mu$
Z = 0.004	5.6×10^{32}	6.3×10^{35}	1.2×10^{34}	5.6×10^{34}	1.9×10^{35}	3.8×10^{35}	7.6×10^{36}	3.7×10^{37}	6.9×10^{37}	7.8×10^{36}	6.8×10^{38}	9.5×10^{38}
Z = 0.016	5.6×10^{32}	2.1×10^{34}	4.2×10^{34}	5.5×10^{34}	4.0×10^{35}	7.8×10^{35}	6.9×10^{36}	4.8×10^{37}	8.9×10^{37}	6.3×10^{36}	7.4×10^{38}	1.0×10^{37}
Z = 0.057	6.3×10^{32}	4.9×10^{34}	9.8×10^{34}	5.5×10^{34}	5.0×10^{35}	9.3×10^{35}	2.3×10^{38}	5.0×10^{37}	9.1×10^{37}	1.7×10^{38}	6.5×10^{38}	8.7×10^{38}
m = 0	1.9×10^{31}	3.2×10^{33}	6.6×10^{33}	8.7×10^{34}	1.1×10^{34}	2.1×10^{34}	1.1×10^{36}	1.0×10^{36}	1.9×10^{36}	1.1×10^{36}	3.5×10^{38}	4.8×10^{38}
m = 2 Zmax = 2	3.5×10^{31}	1.3×10^{32}	2.5×10^{32}	1.1×10^{33}	2.5×10^{34}	4.6×10^{34}	9.8×10^{37}	1.7×10^{36}	3.0×10^{37}	9.3×10^{37}	5.5×10^{38}	7.6×10^{38}
m = 4 Zmax = 2	7.4×10^{31}	4.6×10^{32}	8.9×10^{32}	1.4×10^{33}	6.8×10^{34}	1.3×10^{33}	8.1×10^{37}	3.4×10^{36}	5.8×10^{36}	7.8×10^{37}	8.7×10^{38}	1.2×10^{37}
m = 4 Zmax = 4	7.4×10^{31}	1.4×10^{31}	2.6×10^{31}	1.4×10^{33}	1.5×10^{33}	2.8×10^{33}	8.1×10^{37}	3.7×10^{36}	6.0×10^{36}	7.8×10^{37}	9.8×10^{38}	1.2×10^{37}

the source. The flux of neutrinos with these energies is determined mainly from the luminosity of the highest energy cosmic rays from nearby sources. The estimated flux of neutrinos is given in Table 1.

The method to detect the secondary neutrinos is to search for neutrino induced leptons produced by the charged current processes $\nu_l + N \to l^- + X$[11]. The small-x behavior of the QCD structure functions increases the cross section above $\sim 100\ TeV$[12]. The production rate of the induced leptons is obtained by

$$\frac{dN}{dE_l dX_t} = N_A \int_{E_l} dE_\nu \frac{dN}{dE_\nu}\frac{d\sigma}{dE_l}(E_\nu), \tag{6.1}$$

where dN/dE_ν is the neutrino energy spectrum, N_A is Avogadro's number, X_t is the column density in g/cm^2, E_l is the induced lepton energy, and $d\sigma/dE_l$ is the differential cross section for the charged current processes. Fig.9 shows the flux of the neutrino-induced electrons obtained by (6.1) for a diffuse source model. In order to detect the neutrinos above $10^{16}\ eV$, $\sim 3\times10^{17} g\ sr$ of target is required. Even in the optimistic case of $m = 4$ and $z_{max} = 4.0$, only 5 events/year are expected in this calculation.

§7. Spectrum of the secondary gamma rays

Photons from secondary π^0 decay and secondary electrons produced by the interaction of UHECR with MWB photons produce an electromagnetic cascade[14] in the intergalactic space. The processes consist of four kinds of interaction, pair creation, inverse Compton scattering, electron pair production, and double pair production. The last two channels are higher order

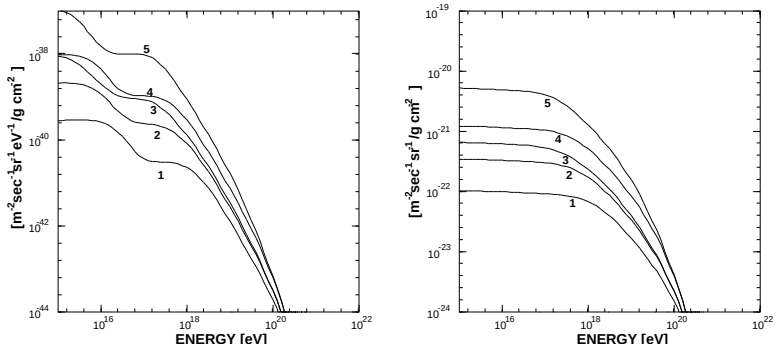

Figure 9: The differential and integral flux of neutrino-induced electrons per unit depth of target material. **1** is for $(m, z_{max}) = (0.0, 2.0)$, **2** $(m, z_{max}) = (2.0, 2.0)$, **3** $(m, z_{max}) = (2.0, 4.0)$, **4** $(m, z_{max}) = (4.0, 2.0)$, and **5** $(m, z_{max}) = (4.0, 4.0)$.

and become important only in the energy region above 10^{19} eV[15]. Cross sections for these channels have been obtained by several authors[16].

To calculate the electromagnetic cascade caused by electrons and gamma rays, we first obtain the number of collisions of electrons or gamma rays with energy E_0 in the cascade, per unit length per unit recoil energy of electrons or gamma rays. The equation for the process is similar to (4.1) for UHECR collisions.

$$\frac{dN}{dLdE} = \frac{1}{4\pi c}\int (1+\cos\theta)\frac{d\sigma}{dE}(s)\frac{dn_\gamma}{dE_\gamma}(s,\theta)\frac{dE_\gamma}{ds}d\Omega ds, \qquad (7.1)$$

where E is the recoil energy of electrons or gamma rays, $d\sigma/dE$ is the differential cross section of the interaction in the cascade, and θ is the collision angle between high energy electrons or gamma rays and MWB photons.

From (7.1), we construct an energy transfer matrix $n(E_i, E_j)$. Each component of the matrix corresponds to the probability of electrons (gamma rays) transferring their energies from E_i to E_j in the cascade after propagation of a step of distance ΔL. Many steps, corresponding to a series matrix multiplication, gives the final transfer matrix which describes the cascade development from a given epoch z to present epoch. After each step of the multiplication, all components of the transfer matrix are recalculated in order to take the adiabatic energy loss into account.

The obtained flux of gamma rays are shown in Fig.10. The normalization is the same as that for the neutrino flux described in the previous section. The flux decreases as the propagation distance or the evolution parameter becomes large. In the energy region above 10^{19} eV, the higher order processes of both electron pair creation ($\gamma_{BB}e \to e^+e^-e$) and double pair creation ($\gamma_{BB}\gamma \to eeee$) become the main processes in the cascade. The mean free

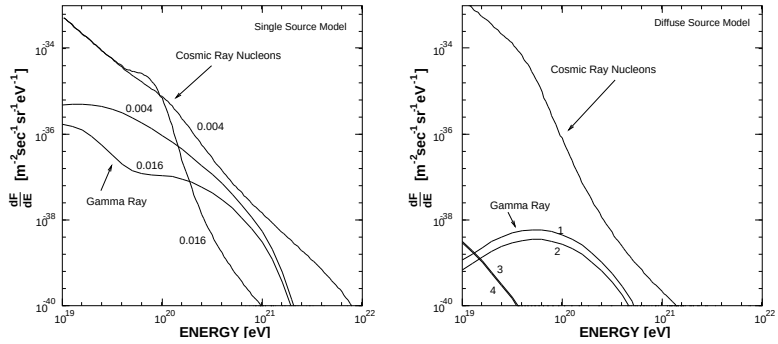

Figure 10: The energy spectra of secondary gamma rays. The red shift z and parameters m, and z_{max} of diffuse sources are given (See key below). The calculated spectra of cosmic ray nucleons are also shown for comparison. **1** is for $(m, z_{max}) = (0.0, 2.0)$, **2** $(m, z_{max}) = (2.0, 2.0)$, **3** $(m, z_{max}) = (2.0, 4.0)$, and **4** $(m, z_{max}) = (4.0, 4.0)$.

path of gamma rays is ~ 100 Mpc above $10^{20}\ eV$ which is much longer than the attenuation length of UHECR. Thus, the gamma ray flux dominates or becomes comparable to the UHECR flux when UHECR are supplied mainly by nearby sources. The gamma ray flux is low, however, if the origin is diffuse-like and the distant sources are the main supplier of UHECR.

§8. Summary and main conclusions

We calculated numerically the propagation effects of UHECR nucleons in the MWB photon field and obtained the flux of both UHECR and secondary particles. Our method of using a Monte-Carlo method enabled us to take into account the kinematics of each interaction with MWB photons, and highlights the broadening in the energy spectrum when the number of interactions of UHECR is few.

From the precise measurement of the shape of the UHECR energy spectrum, we can learn a great deal about the origin of UHECR. The spectra from extragalactic single-like objects have structures depending strongly on propagation distance because of the attenuation of UHECR in the MWB photon field. The spectrum from the sources distributed isotropically has a strong cut off but no bump is created by recoil UHECR. It is difficult to determine the parameters m and z_{max} by measurement of UHECR above $10^{19}\ eV$ alone, because the spectral shape of UHECR above $10^{19}\ eV$ is quite similar between different values of m and z_{max} as shown in Fig.5. The calculated energy spectrum has only a moderate cut off when nearby sources like the Virgo cluster are the main suplier of UHECR above $10^{19}\ eV$. The cut off is much lower in energy for distant sources. The existence of cosmic

rays up tp 10^{20} eV[7),8)] excludes the probability that UHECR are mainly from extremely distant sources.

The flux of the secondary neutrinos is expected to be 10^{-33} to 10^{-31} m^{-2} sec^{-1} sr^{-1} eV^{-1} at 10^{18} eV and 10^{-38} to 10^{-35} m^{-2} sec^{-1} sr^{-1} eV^{-1} at 10^{20} eV depending on the parameters concerned with the origin of UHECR. The flux of neutrinos can be a good probe to estimate the turn-on time, evolution parameter, and the maximum energy of primary UHECR. The flux of the electrons which is induced by the electron neutrinos in the rock or atmosphere is also estimated to study the possibility to detect them. The flux of the induced electrons in the targets is quite low ($\sim 5 \times 10^{-21}$ $m^{-2}\sec^{-1}sr^{-1}/g\ cm^2$). Huge targets of $\sim 3 \times 10^{17} g\ sr$ are needed to detect the showers caused by neutrino-induced electrons at $\sim 5 events/year$. For example, in the deeply penetrating air shower technique, one searches for air showers initiated at much deeper depth than that expected for cosmic ray hadrons. The typical depth of the target atmosphere is $\sim 5000 g/cm^2$, corresponding to the transversed depth of typical horizontally inclined showers. In this case, the detectors need larger than the $\sim 6000 km^2\ sr$ of aperture for the deeply penetrating air showers above 10^{16} eV. If certain AGN's are powerful sources of neutrinos[13)], the combined flux from many AGN's dwarfs even our most optimistic prediction on the flux of neutrinos from UHECR in the energy region below $10^{19} eV$. Even if this direct neutrino production from AGN is included, secondary neutrinos from UHECR propagation dominate over AGN neutrinos above 10^{19} eV.

The flux of secondary gamma rays is only 10^{-38} $m^{-2}\sec^{-1}sr^{-1}eV^{-1}$ when evolutionary effects become important, while it is comparable to the UHECR flux in the case of a single nearby source.

This calculation does not include the possibility that heavy nuclei are the main component of UHECR. Heavy nuclei would suffer photodisintegration. The detailed calculation has been carried out for the single source model[17)]. A modification in the energy spectrum similar to the one shown here for the case of UHECR nucleons would appear. Our calculated results will be applied to the observed result by future up comming experiments[19)] and improve our knowledge of the source of UHECR.

Acknowledgements

The authors are grateful to Professor F.Kakimoto for fruitful discussions. We also wish to thank Professor M.Nagano for support and encouragement at the Institute for Cosmic Ray Research, University of Tokyo. We thank Dr.G.M.Dion for his careful reading of the manuscript. The analysis was carried out on the **FACOM M780** computer of the Institute for Nuclear Study, University of Tokyo.

References

1) K.Greisen, *Phys.Rev.Lett.* **16** (1966), 748.
2) G.T.Zatsepin, and V.A.Kuźmin, *Pisma Zh.Eksp. Teor.Fiz.* **4** (1966), 114.
3) C.T.Hill and D.N.Schramm, *Phys.Rev.D* **31** (1985), 564.
4) V.S.Berezinsky and S.I.Grigor'eva, *Astron.Astrophys.* **199** (1988), 1.
5) Cambridge Bubble Chamber Group, *Phys.Rev.***155** (1967), 1477; T.A.Armstrong *et al., Phys.Rev.D* **5** (1972), 1640; D.O.Caldwell *et al., Phys.Rev.D* **7** (1973), 1362; H.H.Bingham *et al., Phys.Rev.D* **8** (1973), 1277.
6) M.Giler, J.Wdowczyk, A.W.Wolfendale *J.Phys.G:Nucl.Phys.* **6** (1980), 1561; J.Wdowczyk and A.W.Wolfendale *J.Phys.G:Nucl.Phys.* **16** (1990), 1399.
7) M.Nagano *et al., J.Phys.G:Nucl.Phys.* **18** (1992), 423;
8) M.A.Lawrence, R.J.O.Reid and A.A.Watson, *J.Phys.G:Nucl.Phys.* **17** (1991), 733.
9) Dunlop and Peacock, Edinburgh Astron. Preprint.
10) S.Hayakawa, *Phys. Rev.* **108** (1957), 1533.
11) R.M.Baltrusaitis *et al., Phys.Rev.D* **31** (1985), 2192.
12) D.W.Mackey and J.P.Ralston, *Physics Lett.* **167B** (1986), 103; C.Quigg, M.H.Reno, and T.P.Walker, *Phys.Rev.Lett.* **57** (1986), 774; T.K.Gaisser and A.G.Grillo, *Phys.Rev.D* **36** (1987), 2752.
13) *See the useful review and discussion of* S.Barwick *et al., J.Phys.G:Nucl.Phys.* **18** (1992), 225.
14) J.Wdowczyk *et al.*, *J.Phys* **A5** (1972), 1419; W.Michalak, J.Wdowczyk, and A.W.Wolfendale, *J.Phys.G:Nucl.Part.Phys.* **16** (1990), 1917.
15) F.Halzen *et al.*, *Phys.Rev.D* **41** (1990), 342.
16) V.Votruba, *Phys.Rev.* **73** (1948), 1468; J.Rohrlich,*Theory of Photons and Electrons.* (Addison-Wesley Publishing Company 1955); R.W.Brown *et al., Phys.Rev.D* **8**(1973), 3083.
17) J.L.Puget, F.W.Stecker, and J.H.Bredekamp, *Ap.J.* **205** (1976), 638.
18) S.Weinberg, *Gravitation and Cosmology* (Wiley, New York, 1972).
19) E.C.Loh, *Nucl.Phys.B (Proc.Suppl.)* **14A** (1990), 256;
M.Teshima *et al.*, *Nucl.Phys. B* (Proc.Suppl.), **28B** (1992), 169.